JACS
JOURNAL OF THE AMERICAN CHEMICAL SOCIETY

Subscriber access provided by ISTANBUL TEKNIK UNIV

Article

Extensive Backbone Dynamics in the GCAA RNA Tetraloop Analyzed Using C NMR Spin Relaxation and Specific Isotope Labeling

James E. Johnson Jr., and Charles G. Hoogstraten

J. Am. Chem. Soc., **2008**, 130 (49), 16757-16769 • DOI: 10.1021/ja805759z • Publication Date (Web): 17 November 2008

Downloaded from http://pubs.acs.org on February 8, 2009

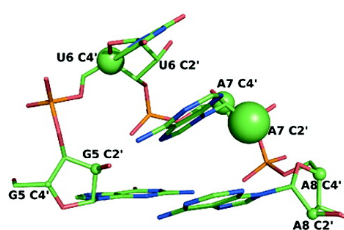

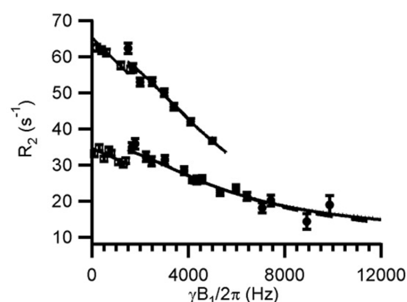

More About This Article

Additional resources and features associated with this article are available within the HTML version:

- Supporting Information
- Access to high resolution figures
- Links to articles and content related to this article
- Copyright permission to reproduce figures and/or text from this article

View the Full Text HTML

ACS Publications
High quality. High impact.

Journal of the American Chemical Society is published by the American Chemical Society. 1155 Sixteenth Street N.W., Washington, DC 20036

J|A|C|S

ARTICLES

Published on Web 11/17/2008

Extensive Backbone Dynamics in the GCAA RNA Tetraloop Analyzed Using ^{13}C NMR Spin Relaxation and Specific Isotope Labeling

James E. Johnson, Jr. and Charles G. Hoogstraten*

Department of Biochemistry and Molecular Biology, Michigan State University, East Lansing, Michigan 48824

Received July 23, 2008; E-mail: hoogstr3@msu.edu

Abstract: Conformational dynamics play a key role in the properties and functions of proteins and nucleic acids. Heteronuclear NMR spin relaxation is a uniquely powerful site-specific probe of dynamics in proteins and has found increasing applications to nucleotide base side chains and anomeric sites in RNA. Applications to the nucleic acid ribose backbone, however, have been hampered by strong magnetic coupling among ring carbons in uniformly ^{13}C-labeled samples. In this work, we apply a recently developed, metabolically directed isotope labeling scheme that places ^{13}C with high efficiency and specificity at the nucleotide ribose C2′ and C4′ sites. We take advantage of this scheme to explore backbone dynamics in the well-studied GCAA RNA tetraloop. Using a combination of CPMG (Carr−Purcell−Meiboom−Gill) and $R_{1\rho}$ relaxation dispersion spectroscopy to explore exchange processes on the microsecond to millisecond time scale, we find an extensive pattern of dynamic transitions connecting a set of relatively well-defined conformations. In many cases, the observed transitions appear to be linked to C3′-endo/C2′-endo sugar pucker transitions of the corresponding nucleotides, and may also be correlated across multiple nucleotides within the tetraloop. These results demonstrate the power of NMR spin relaxation based on alternate-site isotope labeling to open a new window into the dynamic properties of ribose backbone groups in RNA.

Introduction

Along with a precise knowledge of three-dimensional structure, a detailed appreciation of the conformational transitions and equilibrium fluctuations of a protein, nucleic acid, or complex is necessary to achieve an integrated view of molecular function. Due to its ability to probe simultaneously numerous sites throughout the molecule in a nonperturbative fashion, heteronuclear NMR spin relaxation spectroscopy has become a central method to study such time-dependent properties of proteins.[1−7] In RNA systems, conformational dynamics are key to processes including ribozyme catalysis and ligand recognition.[8−12] Spin relaxation studies for ^{15}N and, more commonly, ^{13}C nuclei on nucleotide base side chains have been reported in a number of systems, and anomeric carbon atoms (C1′) have also been analyzed in some cases.[13−31] The powerful technique of ^{13}C relaxation dispersion spectroscopy for analysis of conformational exchange on the microsecond−millisecond time scale has been applied to RNA[20,24,26,31] and DNA.[32] In a complementary technique, isotope labeling schemes that facili-

(1) Kay, L. E.; Torchia, D. A.; Bax, A. *Biochemistry* **1989**, *28*, 8972–8979.
(2) Palmer, A. G., III. *Chem. Rev.* **2004**, *104*, 3623–3640.
(3) Jarymowycz, V. A.; Stone, M. J. *Chem. Rev.* **2006**, *106*, 1624–1671.
(4) Igumenova, T. I.; Frederick, K. K.; Wand, A. J. *Chem. Rev.* **2006**, *106*, 1672–1699.
(5) Palmer, A. G., III.; Massi, F. *Chem. Rev.* **2006**, *106*, 1700–1719.
(6) Mittermaier, A.; Kay, L. E. *Science* **2006**, *312*, 224–228.
(7) Korzhnev, D. M.; Kay, L. E. *Acc. Chem. Res.* **2008**, *41*, 442–451.
(8) Williamson, J. R. *Nat. Struct. Biol.* **2000**, *7*, 834–837.
(9) Leulliot, N.; Varani, G. *Biochemistry* **2001**, *40*, 7947–7956.
(10) Treiber, D. K.; Williamson, J. R. *Curr. Opin. Struct. Biol.* **2001**, *11*, 309–314.
(11) Fedor, M. J.; Williamson, J. R. *Nat. Rev. Mol. Cell Biol.* **2005**, *6*, 399–412.
(12) Al Hashimi, H. M.; Walter, N. G. *Curr. Opin. Struct. Biol.* **2008**, *18*, 321–329.
(13) Williamson, J. R.; Boxer, S. G. *Biochemistry* **1989**, *28*, 2819–2831.
(14) King, G. C.; Harper, J. W.; Xi, Z. *Methods Enzymol.* **1995**, *261*, 436–450.
(15) Gaudin, F.; Paquet, F.; Chanteloup, L.; Beau, J.-M.; Thuong, N. T.; Lancelot, G. *J. Biomol. NMR* **1995**, *5*, 49–58.
(16) Gaudin, F.; Chanteloup, L.; Thuong, N. T.; Lancelot, G. *Magn. Reson. Chem.* **1997**, *35*, 561–565.
(17) Akke, M.; Fiala, R.; Jiang, F.; Patel, D.; Palmer, A. G., III. *RNA* **1997**, *3*, 702–709.
(18) Hall, K. B.; Tang, C. *Biochemistry* **1998**, *37*, 9323–9332.
(19) Boisbouvier, J.; Brutscher, B.; Simorre, J.-P.; Marion, D. *J. Biomol. NMR* **1999**, *14*, 241–252.
(20) Hoogstraten, C. G.; Wank, J. R.; Pardi, A. *Biochemistry* **2000**, *39*, 9951–9958.
(21) Dayie, K. T.; Brodsky, A. S.; Williamson, J. R. *J. Mol. Biol.* **2002**, *317*, 263–278.
(22) Clerte, C.; Hall, K. B. *Biochemistry* **2004**, *43*, 13404–13415.
(23) Showalter, S. A.; Baker, N. A.; Tang, C.; Hall, K. B. *J. Biomol. NMR* **2005**, *32*, 179–193.
(24) Blad, H.; Reiter, N. J.; Abildgaard, F.; Markley, J. L.; Butcher, S. E. *J. Mol. Biol.* **2005**, *353*, 540–555.
(25) Duchardt, E.; Schwalbe, H. *J. Biomol. NMR* **2005**, *32*, 295–308.
(26) Shajani, Z.; Varani, G. *J. Mol. Biol.* **2005**, *349*, 699–715.
(27) Shajani, Z.; Varani, G. *Biopolymers* **2007**, *86*, 348–359.
(28) Shajani, Z.; Drobny, G.; Varani, G. *Biochemistry* **2007**, *46*, 5875–5883.
(29) Duchardt, E.; Nilsson, L.; Schleucher, J. *Nucleic Acids Res.* **2008**, *36*, 4211–4219.
(30) Ferner, J.; Villa, A.; Duchardt, E.; Widjajakusuma, E.; Wohnert, J.; Stock, G.; Schwalbe, H. *Nucleic Acids Res.* **2008**, *36*, 1928–1940.

10.1021/ja805759z CCC: $40.75 © 2008 American Chemical Society

tate solution-state ^{2}H NMR analysis of fast motions on ribose groups have been introduced.[33,34]

Spin relaxation studies of backbone ribose ^{13}C nuclei of RNA have lagged behind those of the nucleotide base side chains due to complications from scalar and dipolar spin−spin couplings within the five-carbon ribose group. For molecules with rotational correlation times (τ_c) less than ~5 ns, accurate measurement of longitudinal autorelaxation rates can be obtained in uniformly labeled samples.[31,32,35,36] At the longer correlation times characteristic of larger systems, however, ^{13}C−^{13}C cross-relaxation effects become highly significant, leading to multiexponential decay for R_1 experiments and potentially serious distortions in heteronuclear NOE data.[35,37] For transverse relaxation, by contrast, scalar (J) couplings between adjacent carbon atoms are the most troublesome sources of error. In CPMG (Carr−Purcell−Meiboom−Gill) R_2 measurements, which are critical to analysis of dynamics on the millisecond time scale, $^{1}J_{CC}$ effects interfere with the refocusing of the $^{1}J_{CH}$ couplings, essentially precluding the use of these experiments.[37] For transverse relaxation under spin-locked conditions ($R_{1\rho}$), distortions arising from transfer between adjacent spins via the Hartmann−Hahn mechanism are possible when adjacent ^{13}C atoms have similar chemical shifts. For the relatively well-dispersed ribose carbon resonances of DNA, such effects can often be neglected.[35] This assumption, however, may be much less valid in RNA systems given the tighter clustering of the ribose spectra. For example, in the lead-dependent ribozyme, the median $\Delta\delta$ between C2′ and C3′ is only 2.6 ppm, and the two chemical shift ranges actually overlap.[38] For relaxation dispersion studies, the possibility of spurious ω_1 dependence of relaxation rates makes Hartmann−Hahn effects a particular concern.

In earlier work, we used comparisons of uniformly and specifically labeled nucleotides adjusted to varying correlation times to determine the effects of ^{13}C−^{13}C interactions on relaxation within the RNA ribose ring.[36] In agreement with other work,[31,32,35] we found that longitudinal relaxation measurements were unaffected up to a correlation time of ~5 ns. At higher correlation times, however, we found significant divergence between R_1 measurements in uniformly and specifically labeled nucleotides, reaching a 2-fold error at a τ_c of 17 ns. Substantial deviations were also found (depending on the resonance and the spin-lock power) between the two labeling patterns in $R_{1\rho}$ measurements. In short, although useful results may be obtained with uniformly labeled nucleotides in some cases, scalar and dipolar one-bond ^{13}C−^{13}C interactions pose a significant barrier to the accurate measurement of relaxation parameters in RNA ribose carbons, especially for R_1 data in systems larger than about 40 nucleotides, for $R_{1\rho}$ data in poorly dispersed RNA systems, and for CPMG transverse relaxation data under most or all circumstances.

Scheme 1. Equilibrium between C3′-endo and C2′-endo Ribose Conformations

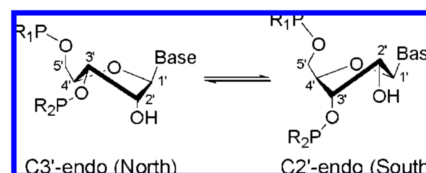

In order to provide a general solution to problems associated with ^{13}C−^{13}C interactions in nucleic acids, we introduced the technique of metabolically directed specific labeling of C2′ and C4′ ribose groups within RNA.[36] In this method, the biosynthetic preparation of labeled nucleotides is modified by the use of an *Escherichia coli* strain deficient in glucose-6-phosphate dehydrogenase (*zwf* genotype) grown on 2-^{13}C-glycerol; the isolation and purification of the resulting nucleotides then proceeds according to standard methods. This scheme produces very high ^{13}C incorporation at C4′ and >80% incorporation at C2′ with essentially no label elsewhere in the sugar.[36] As a biosynthetic technique, alternate-site labeling has dramatic advantages in the commitment of effort and resources over labeling schemes based on full chemical synthesis, and does not suffer from the very substantial loss of sensitivity that accompanies relaxation work performed at natural isotopic abundance.[39,40] For applications to nucleic acids, we expect 2′,4′-$^{13}C_2$ alternate-site labeling to be particularly useful for analysis of the equilibrium between C3′-endo and C2′-endo envelope ribose forms (Scheme 1). These conformations, corresponding in helical regions to A-form and B-form structures, respectively, represent the two energy minima on the pseudorotation cycle for the five-membered ribose ring. Observed ribose conformations in nucleic acids are dominated by these two pucker forms, and NMR J-coupling analyses are consistent with nucleotide sugars existing in solution as either C3′-endo, C2′-endo, or an equilibrium between these two states.[41−44] We therefore hypothesize that longer time scale (μs−ms) dynamics of the ribose backbone, as measured by NMR relaxation dispersion techniques, are dominated by interconversions between these two forms for a particular nucleotide.

GNRA tetraloops (N = any nucleotide; R = G or A) are an important class of well-structured, thermodynamically stable structural motifs in RNA. They are commonly found in rRNA and other natural systems, where they play important roles in constructing RNA tertiary structure.[45−48] Thus, these motifs have been the subject of intense biochemical, biophysical, and

(31) Oberstrass, F. C.; Allain, F. H.; Ravindranathan, S. *J. Am. Chem. Soc.* **2008**, *130*, 12007–12020.
(32) Shajani, Z.; Varani, G. *Biochemistry* **2008**, *47*, 7617–7625.
(33) Vallurupalli, P.; Kay, L. E. *J. Am. Chem. Soc.* **2005**, *127*, 6893–6901.
(34) Vallurupalli, P.; Scott, L.; Hennig, M.; Williamson, J. R.; Kay, L. E. *J. Am. Chem. Soc.* **2006**, *128*, 9346–9347.
(35) Boisbouvier, J.; Wu, Z.; Ono, A.; Kainosho, M.; Bax, A. *J. Biomol. NMR* **2003**, *27*, 133–142.
(36) Johnson, J. E., Jr.; Julien, K. R.; Hoogstraten, C. G. *J. Biomol. NMR* **2006**, *35*, 261–274.
(37) Yamazaki, T.; Muhandiram, D. R.; Kay, L. E. *J. Am. Chem. Soc.* **1994**, *116*, 8266–8278.
(38) Legault, P.; Hoogstraten, C. G.; Metlitzky, E.; Pardi, A. *J. Mol. Biol.* **1998**, *284*, 325–335.
(39) Isaacs, R. J.; Rayens, W. S.; Spielmann, H. P. *J. Mol. Biol.* **2002**, *319*, 191–207.
(40) Nielsen, K. E.; Spielmann, H. P. *J. Am. Chem. Soc.* **2005**, *127*, 15273–15282.
(41) Altona, C.; Sundaralingam, M. *J. Am. Chem. Soc.* **1972**, *94*, 8205–8212.
(42) Saenger, W. *Principles of Nucleic Acid Structure*; Springer-Verlag: New York, 1984.
(43) Van de Ven, F. J.; Hilbers, C. W. *Eur. J. Biochem.* **1988**, *178*, 1–38.
(44) Wijmenga, S. S.; Mooren, M. M. W.; Hilbers, C. W. In *NMR of Macromolecules: A Practical Approach*; Roberts, G. C. K., Ed.; Oxford University Press: Oxford, 1993; pp 217−288.
(45) Woese, C. R.; Winker, S.; Gutell, R. R. *Proc. Natl. Acad. Sci. U.S.A.* **1990**, *87*, 8467–8471.
(46) Wyatt, J. R.; Tinoco, I., Jr. In *The RNA World: The Nature of Modern RNA Suggests a Prebiotic RNA World*; Gesteland, R. F., Atkins, J. F., Eds.; Cold Spring Harbor Laboratory Press: Plainview, NY, 1993; pp 465−496.

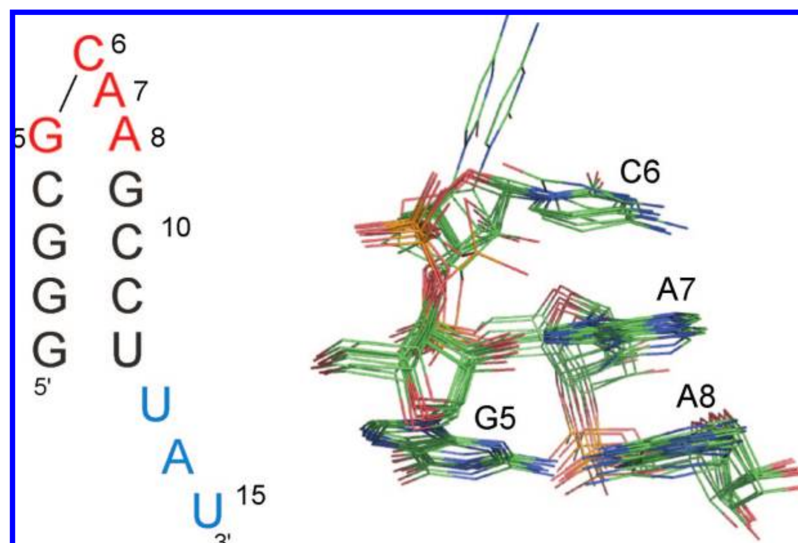

Figure 1. The GCAA helix-tetraloop. (Left) Secondary structure of the construct used in these studies. Tetraloop residues are in red, and the unstructured 3′ tail is in blue. (Right) Superimposition of 10 NMR structures of tetraloop residues 5−8 of the identical construct (pdb code 1ZIH).[53] As is general for the GNRA class of tetraloops, the first nucleotide (G5) stacks on the 5′ strand of the adjoining helix, whereas the three succeeding nucleotides stack on the 3′ strand with Watson−Crick faces accessible to solvent. The family of NMR structures suggests sampling of an unstacked conformation for the apical residue C6, observed in 2 of the 10 reported conformers.

structural studies,[49−61] rendering them an excellent model system for careful NMR characterization of conformational dynamics. For the present purpose, comparisons of novel spin relaxation measurements of the ribose group with detailed preexisting data are invaluable in validating the usefulness of the novel labeling technology. In this work, therefore, we have analyzed the dynamics of the GCAA variant of the GNRA motif (Figure 1) with a comprehensive set of NMR relaxation experiments on the C2′ and C4′ resonances using alternate-site labeled nucleotides. We find that ribose groups in the tetraloop are relatively rigid on the ps−ns time scale but show an extensive pattern of conformational exchange on the μs−ms time scale. These results point the way to the use of this technology for detailed studies of the relationship between dynamics and function in ribozymes, ligand-binding RNAs, and other systems of interest.

Experimental Section

RNA Synthesis and Purification. Nucleoside triphosphates were prepared from cultures of *E. coli* strain K12-15-16, which carries a mutation in the glucose-6-phosphate dehydrogenase gene, grown on 2-^{13}C-glycerol.[36] The 15-nucleotide GCAA hairpin-tetraloop was transcribed *in vitro* from the resulting 2′,4′-$^{13}C_2$ ribonucleotides using recombinant T7 RNA polymerase and a synthetic DNA template.[62−65] Transcribed RNA was purified using denaturing polyacrylamide electrophoresis on a Bio-Rad model 491 prep cell, desalted using G-25 Sephadex, and resuspended to a final concentration of 1.2 mM in 99.96% D_2O, 10 mM sodium phosphate buffer pH 6.8, 100 mM NaCl, 200 μM EDTA in a 280 μL NMR tube (Shigemi).

NMR Spectroscopy. Spectra were acquired on Varian UnityINOVA 600 MHz and Bruker Avance 900 MHz spectrometers. At 900 MHz, a cryogenically cooled probe (Bruker TCI) was used to acquire R_1, heteronuclear NOE, and CPMG data. All other data used room-temperature probes. Resonance assignments were taken from those reported by Pardi and co-workers.[53] For analysis of fast dynamics, minor variations of published pulse sequences were used to acquire ^{13}C R_1, $R_{1\rho}$, and heteronuclear NOE data at 25 °C, with a 3 kHz applied spin-lock field (ω_1) used for $R_{1\rho}$.[37] Dynamics on the μs−ms time scale were analyzed using relaxation dispersion curves consisting of relaxation-compensated CPMG data as a function of interpulse spacing $2\tau_{cp}$ and on- and off-resonance $R_{1\rho}$ data as a function of applied spin-lock field and resonance offset, respectively.[37,66−70] Dispersion data were obtained at 15, 20, 25, and 35 °C at 600 MHz (150 MHz ^{13}C) and 25 °C at 900 MHz (225 MHz ^{13}C). For CPMG experiments, τ_{cp} typically varied from

(47) Cate, J.; Gooding, A. R.; Podell, E.; Zhou, K.; Golden, B. L.; Kundrot, C. E.; Cech, T. R.; Doudna, J. A. *Science* **1996**, *273*, 1678–1685.
(48) Ban, N.; Nissen, P.; Hansen, J.; Moore, P. B.; Steitz, T. A. *Science* **2000**, *289*, 905–920.
(49) Antao, V. P.; Tinoco, I., Jr. *Nucleic Acids Res.* **1992**, *20*, 819–824.
(50) Heus, H. A.; Pardi, A. *Science* **1991**, *253*, 191–194.
(51) SantaLucia, J.; Kierzek, R.; Turner, D. H. *Science* **1992**, *256*, 217–219.
(52) Jucker, F. M.; Pardi, A. *RNA* **1995**, *1*, 219–222.
(53) Jucker, F. M.; Heus, H. A.; Yip, P. F.; Moors, E. H. M.; Pardi, A. *J. Mol. Biol.* **1996**, *264*, 968–980.
(54) Menger, M.; Eckstein, F.; Porschke, D. *Biochemistry* **2000**, *39*, 4500–4507.
(55) Sorin, E. J.; Engelhardt, M. A.; Herschlag, D.; Pande, V. S. *J. Mol. Biol.* **2002**, *317*, 493–506.
(56) Sarzynska, J.; Nilsson, L.; Kulinski, T. *Biophys. J.* **2003**, *85*, 3445–3459.
(57) Sorin, E. J.; Rhee, Y. M.; Nakatani, B. J.; Pande, V. S. *Biophys. J.* **2003**, *85*, 790–803.
(58) Sorin, E. J.; Rhee, Y. M.; Pande, V. S. *Biophys. J.* **2005**, *88*, 2516–2524.
(59) Correll, C. C.; Swinger, K. *RNA* **2003**, *9*, 355–363.
(60) Trantirek, L.; Caha, E.; Kaderavek, P.; Fiala, R. *J. Biomol. Struct. Dyn.* **2007**, *25*, 243–252.
(61) Zhao, L.; Xia, T. *J. Am. Chem. Soc.* **2007**, *129*, 4118–4119.
(62) Batey, R. T.; Inada, M.; Kujawinski, E.; Puglisi, J. D.; Williamson, J. R. *Nucleic Acids Res.* **1992**, *20*, 4515–4523.
(63) Nikonowicz, E. P.; Sirr, A.; Legault, P.; Jucker, F. M.; Baer, L. M.; Pardi, A. *Nucleic Acids Res.* **1992**, *20*, 4507–4513.
(64) Batey, R. T.; Battiste, J. L.; Williamson, J. R. *Methods Enzymol.* **1995**, *261*, 300–322.
(65) Kao, C.; Zheng, M.; Rüdisser, S. *RNA* **1999**, *5*, 1268–1272.
(66) Loria, J. P.; Rance, M.; Palmer, A. G., III. *J. Am. Chem. Soc.* **1999**, *121*, 2331–2332.
(67) Meekhof, A. E.; Freund, S. M. *J. Biomol. NMR* **1999**, *14*, 13–22.
(68) Mulder, F. A.; Hon, B.; Mittermaier, A.; Dahlquist, F. W.; Kay, L. E. *J. Am. Chem. Soc.* **2002**, *124*, 1443–1451.
(69) Mulder, F. A. A.; de Graaf, R. A.; Kaptein, R.; Boelens, R. *J. Magn. Reson.* **1998**, *131*, 351–357.
(70) Mulder, F. A. A.; Mittermaier, A.; Hon, B.; Dahlquist, F. W.; Kay, L. E. *Nat. Struct. Biol.* **2001**, *8*, 932–935.

180 to 2500 μs, corresponding to effective spin-lock powers ω_{eff} of ~1400 to 80 Hz. For on-resonance $R_{1\rho}$ experiments, ω_1 varied from 1.5 to 6.0 kHz at 600 MHz and from 1.5 to 5.2 kHz at 900 MHz. At 600 MHz, a single irradiation offset intermediate between the C2′ and C4′ spectral regions was used; at 900 MHz, separate data sets were acquired with the carrier centered on the C2′ and C4′ regions independently. Off-resonance $R_{1\rho}$ experiments (600 MHz only) were performed at a constant ω_1 of 3 kHz with resonance offsets ranging from 3.5 to 10 kHz. For all experiments, the typical total relaxation time was 84 ms, with curves reacquired at shorter delays as necessary for fast-relaxing resonances. At 15 °C, the off-resonance $R_{1\rho}$ experiment was omitted on the basis of inspection of the on-resonance curves (see Results). At 20 °C, CPMG data were not collected.

Data Analysis. NMR spectra were processed using Felix 2002 with a 3 Hz exponential line broadening in t_2 and extension by 20% using linear prediction followed by cosine-squared apodization in t_1. Peak intensities were integrated in Felix and exported to Igor Pro 5.0.4. Longitudinal and transverse ^{13}C relaxation rates were extracted by fitting the integrated peaks to a two-parameter single exponential decay. Offset-corrected $R_{1\rho}$ values were extracted using $R_{1\rho}^{obs} = R_1 \cos^2\theta + R_{1\rho}\sin^2\theta$, where $\theta = \tan^{-1}(\omega_1/\Omega)$ is the angle of the spin-lock axis from the z axis, ω_1 is the spin-lock power, and Ω is the resonance offset.[2,5] Reported heteronuclear NOE values are the ratio between cross-peak integrals observed with and without applied ^{1}H saturation.

Motional disorder on the ps−ns time scale was analyzed with the standard model-free approach[1,71,72] using the implementation of Palmer and co-workers in Modelfree 4.15.[73,74] Model-free analysis was performed using relaxation parameters measured at 600 MHz, for which a more complete data set was available. A C−H distance of 0.11 nm, chemical shift anisotropy (CSA) values of 26.6 ppm and 91.7 ppm for C2′ and C4′ spins, respectively,[75] and an isotropic model for global tumbling were used. Fitting to an axially symmetric tumbling model did not give a statistically significant improvement in agreement with the data. Using the protocol and statistical criteria devised by Palmer and co-workers,[74] we chose among models invoking various combinations of the internal motion order parameter S^2, internal correlation time τ_e, and exchange contribution to transverse relaxation R_{ex}. Of the total of 22 resonances analyzed, 11 could be satisfactorily fit using S^2 alone, indicating an internal correlation time of ~10 ps or less, 2 additionally required an explicit τ_e, 6 (comprising 6 of the 8 resonances within the tetraloop) additionally required R_{ex}, and 3 (including one resonance from the tetraloop) required all three parameters. The C2′ carbon of residue G1, C2′ of U13, and C4′ of U13, all in terminal or unstructured regions distal from the tetraloop, could not be fit by any tested model and are omitted from the reported results. After model selection was complete, a final optimization was performed in which global and local motional parameters were allowed to vary simultaneously. The resulting isotropic correlation time for overall tumbling was 3.00 ns ± 0.03 ns, in good agreement with a value recently reported from analysis of nucleotide base ^{13}C data in a 14-nucleotide GCAA construct.[60]

For dispersion curves, R_2^{CPMG} and $R_{1\rho}^{obs}$ rates were calculated from $1/T \times \ln(I(T)/I_o)$, where $I(T)$ is the measured intensity at relaxation delay T and I_o is the intensity for a reference spectrum with zero relaxation delay.[70,76−78] Offset-corrected $R_{1\rho}$ values were extracted as described above using R_1 values from Figure 3. Errors were estimated from data at a single ω_1 or τ_{cp} value repeated three times or were adjusted to a minimum of 2%. Motional parameters were extracted by simultaneous fitting of all data for a single resonance at a given temperature to eqs 3 and 4 (see below). Global fitting of motional parameters to data from multiple resonances was performed as appropriate. The use of the fast-exchange approximation for CPMG fitting was justified *post hoc* by inspection of the extracted exchange rate constants, all of which are much greater than the expected chemical shift variations upon ribose repuckering.[79−81] More rigorously, we calculated the scaling factor α of Palmer and co-workers:

$$\alpha = \frac{\beta_2 + \beta_1}{\beta_2 - \beta_1}\frac{R_{ex2} + R_{ex1}}{R_{ex2} - R_{ex1}} \quad (1)$$

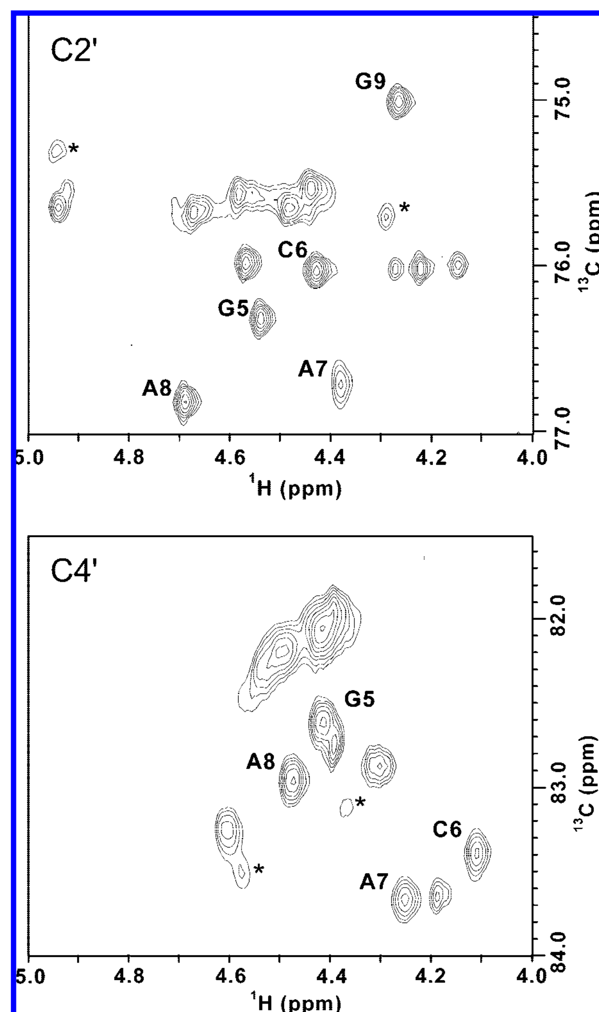

Figure 2. Regions of a ^{1}H−^{13}C HSQC spectrum of a 2′,4′-^{13}C$_2$-labeled GCAA tetraloop corresponding to C2′−H2′ peaks (top) and C4′−H4′ peaks (bottom). Since this spectrum was obtained in nonconstant time mode, the lack of multiplet structure in the ^{13}C dimension demonstrates the effectiveness of the site-directed labeling pattern. Asterisks indicate weak resonances assigned to heterogeneous termini in the RNA transcript.

(71) Lipari, G.; Szabo, A. *J. Am. Chem. Soc.* **1982**, *104*, 4546–4559.
(72) Lipari, G.; Szabo, A. *J. Am. Chem. Soc.* **1982**, *104*, 4559–4570.
(73) Palmer, A. G.; Rance, M.; Wright, P. E. *J. Am. Chem. Soc.* **1991**, *113*, 4371–4380.
(74) Mandel, A. M.; Akke, M.; Palmer, A. G., III. *J. Mol. Biol.* **1995**, *246*, 144–163.
(75) Bryce, D. L.; Grishaev, A.; Bax, A. *J. Am. Chem. Soc.* **2005**, *127*, 7387–7396.
(76) Skrynnikov, N. R.; Dahlquist, F. W.; Kay, L. E. *J. Am. Chem. Soc.* **2002**, *124*, 12352–12360.
(77) Mulder, F. A. A.; Hon, B.; Mittermaier, A.; Dahlquist, F. W.; Kay, L. E. *J. Am. Chem. Soc.* **2002**, *124*, 1443–1451.
(78) Kay, L. E. *J. Magn. Reson.* **2005**, *173*, 193–207.
(79) Ebrahimi, M.; Rossi, P.; Rogers, C.; Harbison, G. S. *J. Magn. Reson.* **2001**, *150*, 1–9.
(80) Dejaegere, A. P.; Case, D. A. *J. Phys. Chem. A* **1998**, *102*, 5280–5289.
(81) Fischer, J. T.; Reinscheid, U. M. *Eur. J. Org. Chem.* **2006**, *2006*, 2074–2080.

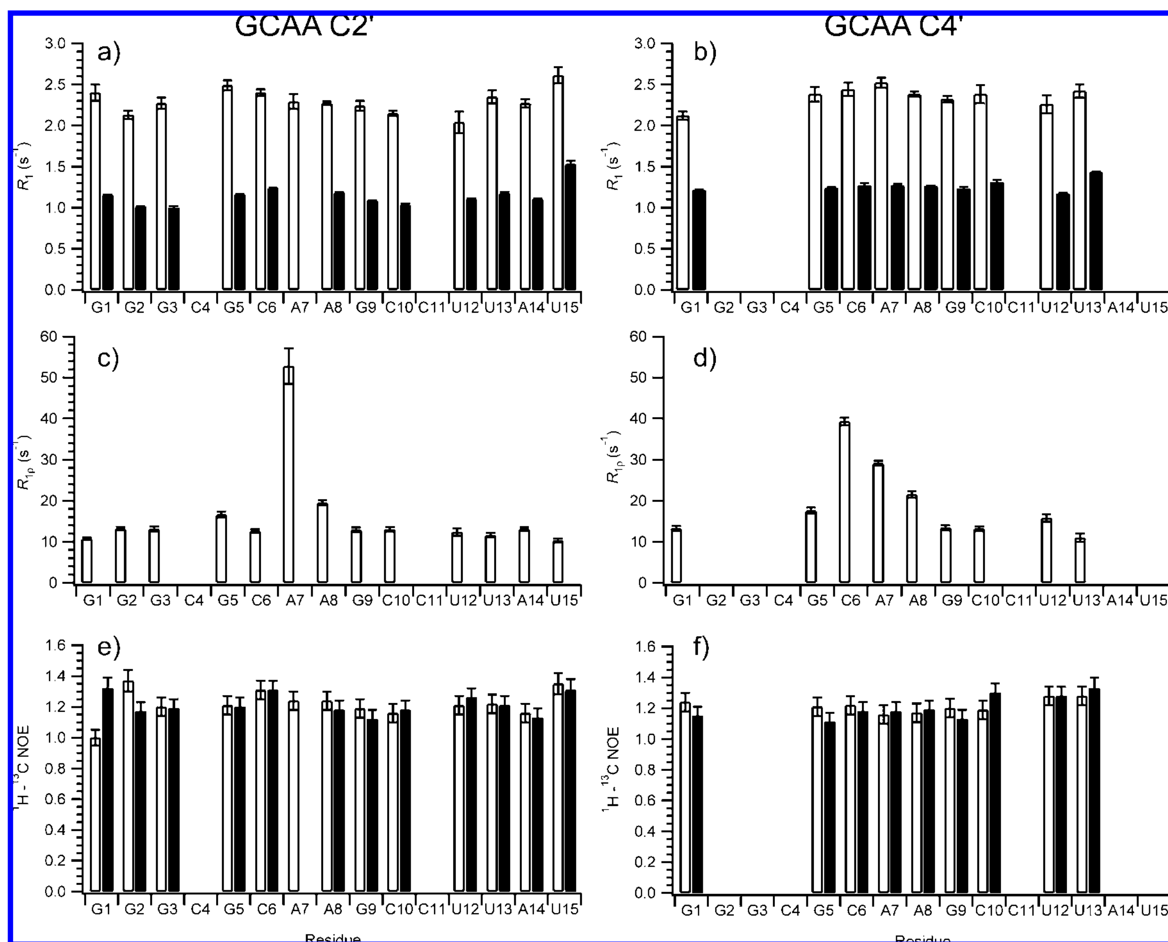

Figure 3. Relaxation parameters in the GCAA tetraloop for C2′ and C4′ resonances. Data for R_1 (a,b), $R_{1\rho}$ (c,d) and the {^{1}H}−^{13}C NOE (e,f) are shown. Open and shaded bars are data from 600 and 900 MHz (150 and 225 MHz ^{13}C), respectively.

where B_1 and B_2 are the magnetic field strengths for the measured values of R_{ex1} and R_{ex2}.[82] For all resonances that could be analyzed at both 600 and 900 MHz, the value of α exceeded 1.7, consistent with behavior in the fast-exchange limit.[82] For A7 C2′, 900 MHz data were unavailable, and the α-value analysis could not be performed.

Results

The GCAA Tetraloop. Figure 2 shows the H2′/C2′ and H4′/C4′ regions of a 600 MHz ^{1}H−^{13}C heteronuclear single-quantum coherence (HSQC) spectrum of a GCAA tetraloop specifically labeled at carbons C2′ and C4′ of the ribose ring. Reasonably well-dispersed spectra are obtained, with 13 of 15 C2′ and 9 of 15 C4′ resonances sufficiently resolved for relaxation analysis, including all eight resonances from the tetraloop nucleotides G5−A8. The broadening of A7 C2′ due to rapid transverse relaxation is clearly visible. At 900 MHz, this peak was broadened beyond detection, and the resonance could therefore only be analyzed at 600 MHz.

The Tetraloop is Well Ordered on the Picosecond−Nanosecond Timescale. Figure 3 reports 25 °C R_1 and heteronuclear NOE data at 600 and 900 MHz and $R_{1\rho}$ data at 600 MHz for ribose C2′ and C4′ resonances in the GCAA tetraloop. Structural disorder on the ps−ns time scale would be expected to result in an increase in R_1 and the heteronuclear NOE and a decrease in R_2. (Due to the opposing signs of the gyromagnetic ratios for ^{13}C and ^{15}N, the variation in the {^{1}H}–X NOE with local correlation time is opposite in sense and smaller in magnitude for ^{13}C than for the more familiar {^{1}H}−^{15}N NOE). For nonterminal residues in double-helical regions (G2-C4 and G9-U12), only minor or occasional variations from uniform behavior for each carbon type are observed, as expected for a rigid structure. At both 600 and 900 MHz, the values of R_1 are noticeably more uniform across the RNA sequence for C4′ than for C2′. The reason for this effect is unclear. For tetraloop residues (G5-A8), small increases in R_1 and NOE values are observed for C2′ atoms only, suggestive of minor structural disorder for the ribose backbone in these regions. For transverse relaxation $R_{1\rho}$, the situation is very different, as the error bars on relaxation rates for seven of the eight resonances in the GCAA tetraloop itself are outside the range of values obtained in helical regions, suggesting substantial contributions of chemical exchange on the μs−ms time scale to transverse relaxation. The exception is C6 C2′, which shows $R_{1\rho}$ typical of helical residues.

To quantify disorder on the ps−ns time scale further, we applied the "model-free" formalism of Lipari and Szabo to the data acquired at 600 MHz.[71,72] The results of this analysis are shown in Table 1 and Figure 4 as the generalized order parameter S^2 and, as appropriate, the correlation time for internal motion τ_e and/or the exchange contribution to transverse relaxation R_{ex} (see Experimental Section).[1,71,72] For the most

(82) Millet, O.; Loria, J. P.; Kroenke, C. D.; Pons, M.; Palmer, A. G. *J. Am. Chem. Soc.* **2000**, *122*, 2867–2877.

Table 1. Model-Free Analysis of Picosecond−Nanosecond Motion Using 600 MHz Data

resonance[a]	S^2	τ_e, ps	R_{ex}, s^{-1}
G2 C2′	0.808 ± 0.044	69.2 ± 19.0	2.00 ± 0.67
G3 C2′	0.973 ± 0.023		
G5 C2′[b]	0.903 ± 0.038	892.4 ± 291.2	3.84 ± 0.79
C6 C2′	0.901 ± 0.028	266.0 ± 83.8	
A7 C2′	0.984 ± 0.027		39.5 ± 4.2
A8 C2′	0.975 ± 0.011		6.28 ± 0.64
G9 C2′	0.960 ± 0.022		
C10 C2′	0.926 ± 0.014		
U12 C2′	0.892 ± 0.042		
A14 C2′	0.972 ± 0.017		
U15 C2′	0.709 ± 0.041	459.6 ± 108.3	
G1 C4′	0.815 ± 0.018		
G5 C4′	0.903 ± 0.036		3.57 ± 0.92
C6 C4′	0.926 ± 0.030		24.9 ± 1.0
A7 C4′	0.956 ± 0.023		14.2 ± 0.7
A8 C4′	0.903 ± 0.014		7.47 ± 0.86
G9 C4′	0.878 ± 0.015		
C10 C4′	0.875 ± 0.028		
U12 C4′	0.792 ± 0.049	40.3 ± 20.5	3.31 ± 1.19

[a] No satisfactory model could be fit for G1 C2′, U13 C2′, and U13 C4′ using the combinations of S^2, τ_e, and R_{ex} tested. As these residues are at the 5′-terminus or in the 3′-unstructured tail, and thus of little relevance to the goals of the study, further detailed analysis was not attempted. [b] This resonance could only be satisfactorily fit by allowing a τ_e value of ~30% of the isotropic correlation time, in violation of the limits of validity of the model-free approach ($\omega\tau_e = 0.67$ for $\omega = \omega_C + \omega_H$).[71,72] Results should be interpreted with caution.

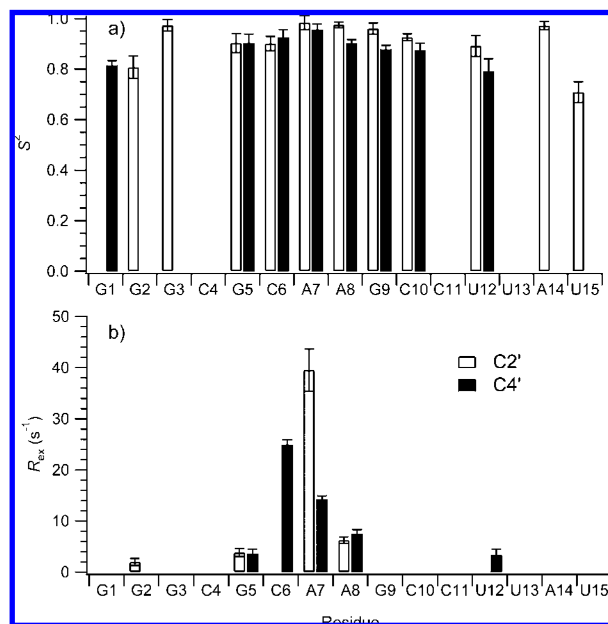

Figure 4. Results of an analysis of relaxation data at 600 MHz using the model-free formalism. (a) Generalized order parameter S^2; (b) exchange contribution to transverse relaxation R_{ex}. Open bars are C2′ and shaded are C4′. A few resonances additionally required the use of an explicit internal correlation time τ_e for successful fitting, not shown here (Table 1).

part, residues showing extensive disorder on fast time scales (low S^2) are found in the terminus of the helix and in the unpaired 3′ tail. The four lowest values of S^2 are calculated for G1 C4′, G2 C2′, U12 C4′, and U15 C2′, as might be expected based on helical fraying and disorder within the single-stranded region. An intriguing exception is A14 C2′, which has an S^2 value among the highest in the molecule despite being located in the penultimate nucleotide in the 3′-tail. The presence of some residual stacking interactions for the corresponding purine ring is possible; alternatively, this ribose may undergo pucker conversion or other dynamics on a time scale intermediate between those reflected in R_{ex} and in S^2 (i.e., the ns−μs regime) and/or segmental dynamics coupled to the overall tumbling of the molecule.[83−86] For U13, the model-free calculations failed to converge for either resonance for the parameter combinations tested, and the C4′ heteronuclear NOE value is the highest in the molecule for this atom type, consistent with the existence of complex dynamics on more than one time scale at the transition from the helix to the unpaired tail.

In the main part of the helix and the tetraloop, the order parameters for a given type of carbon are high and uniform, indicating a lack of structural disorder. This result is consistent with the well-structured and thermodynamically stable nature of the system. We note that relative values of S^2 obtained for the two carbon types are strongly dependent on the values of the chemical shift anisotropy parameter used (data not shown). The values of CSA used here have strong experimental support for rigid A-form helices.[75] We nevertheless suggest that rigorous interpretation of relative order parameters between C2′ and C4′ resonances for a given nucleotide would depend on a careful consideration of the values and relative orientation of the C−H bond vector and the CSA tensor for various states of the ribose ring, which is beyond the scope of the present work.[30]

By contrast, the derived values of R_{ex} show a wide distribution along the RNA sequence, indicating strong, localized contributions from thermally activated exchange processes on the μs−ms time scale. Significant values of R_{ex} are concentrated in the GCAA tetraloop itself, indicating substantial backbone conformational dynamics in this region that contrast with a single ribose conformation within double-stranded regions. The largest exchange contributions are within the capping residues C6 and A7, which also show the greatest degree of conformational averaging in *J*-coupling analysis.[53] Due to the quadratic dependence of R_{ex} on static field in the fast exchange limit, the strong exchange effect at A7 C2′ led to a lack of useful relaxation data for this resonance in the 900 MHz spectrometer, emphasizing the importance of the use of a variety of field strengths for a comprehensive analysis of conformational dynamics. Contributions to relaxation rates from R_{ex} terms are examined in more detail below using relaxation dispersion techniques.

Utility of Multiple Data Sets To Analyze Conformational Exchange. Two-site exchange on the μs−ms time scale may be analyzed rigorously by transverse spin relaxation performed under either repeated spin−echo (CPMG) or spin-lock conditions, denoted R_2^{CPMG} and $R_{1\rho}$, respectively, as a function of the effective B_1 field applied. This approach eliminates potential spurious R_{ex} terms arising from anisotropic motional tumbling or other errors and also allows a quantitative analysis of the time scale and related parameters describing the observed exchange. For either type of experiment, the presence of exchange contributes an additional term R_{ex} to the relaxation rate observed in the absence of exchange, R_2^0 or $R_{1\rho}^0$:[2,5,87−89]

(83) Hansen, A. L.; Al Hashimi, H. M. *J. Am. Chem. Soc.* **2007**, *129*, 16072–16082.
(84) Getz, M. M.; Andrews, A. J.; Fierke, C. A.; Al Hashimi, H. M. *RNA* **2007**, *13*, 251–266.
(85) Zhang, Q.; Al Hashimi, H. M. *Nat. Methods* **2008**, *5*, 243–245.
(86) Meints, G. A.; Miller, P. A.; Pederson, K.; Shajani, Z.; Drobny, G. *J. Am. Chem. Soc.* **2008**, *130*, 7305–7314.
(87) Deverell, C.; Morgan, R. E.; Strange, J. H. *Mol. Phys.* **1970**, *18*, 553–559.

$$R_2^{\mathrm{CPMG}} = R_2^{\ 0} + R_{\mathrm{ex}}$$
$$R_{1\rho} = R_{1\rho}^{\ 0} + R_{\mathrm{ex}} \tag{2}$$

For CPMG experiments in the fast-exchange limit, R_{ex} depends on the interpulse spacing for the spin−echo sequence $2\tau_{cp}$ according to:

$$R_{\mathrm{ex}} = \frac{p_a p_b (\Delta\omega)^2}{k_{\mathrm{ex}}}\left(1 - \frac{\tanh(k_{\mathrm{ex}}\tau_{\mathrm{cp}})}{k_{\mathrm{ex}}\tau_{\mathrm{cp}}}\right) \tag{3a}$$

where p_a and p_b are the populations of the two exchanging states, $\Delta\omega$ is the chemical shift difference between the states for the resonance considered, $k_{ex} = k_1 + k_{-1}$ is the exchange rate constant, and k_1 and k_{-1} are the forward and reverse rate constants for the conversion of state A to B, respectively. For purposes of comparison with $R_{1\rho}$ data, the effective B_1 field may be taken as:

$$\omega_{\mathrm{eff}} = \frac{1}{4\tau_{\mathrm{cp}}} \tag{3b}$$

For transverse relaxation in the fast-exchange limit under spin-lock conditions ($R_{1\rho}$), the exchange contribution is given by

$$R_{\mathrm{ex}} = p_a p_b (\Delta\omega)^2 \frac{k_{\mathrm{ex}}}{\omega_{\mathrm{eff}}^{\ 2} + k_{\mathrm{ex}}^{\ 2}} \tag{4}$$

where the effective field ω_{eff} is the resultant of the applied spin-lock field ω_1 and the resonance offset Ω:

$$\omega_{\mathrm{eff}} = \sqrt{\omega_1^{\ 2} + \Omega^2} \tag{5}$$

For $R_{1\rho}$ experiments, the dependence of R_{ex} on the effective field can thus be determined by either varying ω_1 at a constant offset (the "on-resonance" experiment) or varying resonance offset at a constant ω_1 (the "off-resonance" experiment). For both CPMG and $R_{1\rho}$ experiments in the fast-exchange limit, the parameters that can be extracted from the data are k_{ex}, the product $p_a p_b(\Delta\omega)^2$, abbreviated as Φ_{ex}, and the appropriate relaxation rate in the absence of exchange, R_2^0 or $R_{1\rho}^0$. If multiple datasets are combined, k_{ex} is constant for various types of data and multiple static fields, whereas Φ_{ex} is constant between CPMG and $R_{1\rho}$ and varies predictably with static field according to $(\Delta\omega)^2$.

At a given ω_{eff}, CPMG and $R_{1\rho}$ experiments are generally expected to give very similar quantitative results, and on- and off-resonance $R_{1\rho}$ data should be identical. The utility of acquiring multiple types of data, therefore, does not arise from the ability to perform multiple types of measurements at any given ω_{eff}, but from the different ranges of ω_{eff} accessible using each experimental technique. These topics are discussed in more detail in the Supporting Information. For the current study, we generally acquired CPMG data from ω_{eff} values of 80 to 1400 Hz, on-resonance $R_{1\rho}$ from 1.5 kHz to 6.0 kHz, and off-resonance $R_{1\rho}$ from 4.6 kHz to 10.4 kHz. Finally, it has also been shown that data at multiple static magnetic fields are of great utility in successfully defining exchange parameters.[2,90]

Extensive Microsecond-Scale Ribose Conformational Exchange in Tetraloop Residues. For a comprehensive analysis of μs−ms conformational exchange processes in the GCAA tetraloop at 25 °C, we combined ^{13}C CPMG and on- and off-resonance $R_{1\rho}$ experiments in a 600 MHz spectrometer (150 MHz ^{13}C) with CPMG and on-resonance $R_{1\rho}$ data at 900 MHz (225 MHz ^{13}C). Within helical regions, we see minor but statistically significant dispersion effects, in 900 MHz data only, at G9 C2′ and G3 C2′. We attribute exchange at G9 C2′ to established dynamic processes involving the base of A8,[20,60] since the ring-current shift from this base noticeably affects the observed chemical shift for G9 C2′ (Figure 2.)[53] In contrast, substantial dispersion effects are observed at both fields for seven of the eight tetraloop resonances, as seen in Figure 5. This result agrees completely with the necessity to invoke R_{ex} in the model-free analysis of the same seven resonances (Figure 4; Table 1). For C6 C2′ (Figure 6c), no dispersion is observed apart from that typical for helical residues (see above), again consistent with the model-free results. The slight increase seen

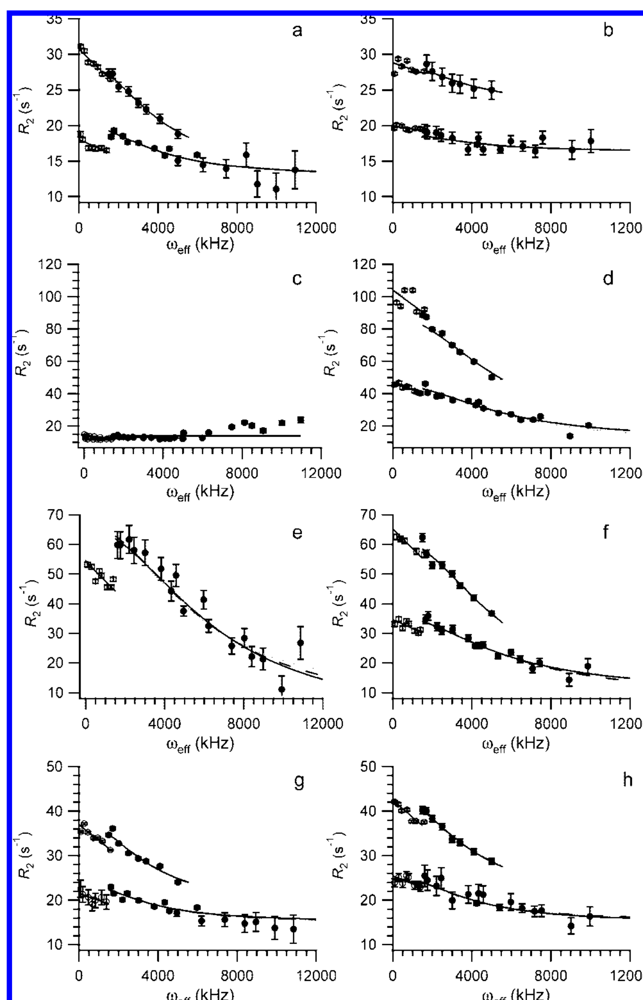

Figure 5. Relaxation dispersion experiments in the GCAA tetraloop. CPMG (open symbols) and on- and off-resonance $R_{1\rho}$ (solid symbols) data are shown for C2′ and C4′ resonances respectively of G5 (a,b), C6 (c,d), A7 (e,f), and A8 (g,h). All corrections for resonance offset have been applied. Upper traces represent data at 900 MHz (225 MHz ^{13}C) and lower traces at 600 MHz (150 MHz ^{13}C) except in the case of A7 C2′, for which data at 900 MHz were unavailable due to fast relaxation. For C6 C2′, a horizontal-line fit to the data is shown. Otherwise, solid lines denote simultaneous fits of all data for the corresponding resonance to eqs 3 and 4, dashed lines (for G5, A7, and A8) denote simultaneous fits to C2′ and C4′ results for a particular residue, and dotted lines represent global fits of all data for either C6 and C7 (apical residues) or G5 and A8 (closing base pair). In many cases, dashed and/or dotted lines are not visible due to coincidence with the solid lines representing resonance-specific fits.

(88) Bloom, M.; Reeves, L. W.; Wells, E. J. *J. Chem. Phys.* **1965**, *42*, 1615–1624.
(89) Palmer, A. G.; Kroenke, C. D.; Loria, J. P. *Methods Enzymol.* **2001**, *339*, 204–238.
(90) Kovrigin, E. L.; Kempf, J. G.; Grey, M. J.; Loria, J. P. *J. Magn. Reson.* **2006**, *180*, 93–104.

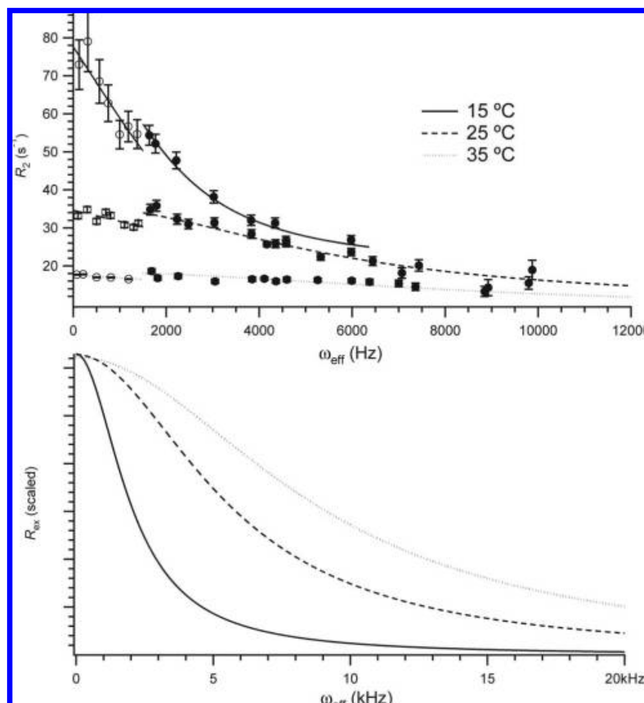

Figure 6. Temperature dependence of relaxation dispersion for A7 C4′. (Top) ^{13}C CPMG (open symbols) and $R_{1\rho}$ (solid symbols) data acquired at 15 °C, 25 °C, and 35 °C and 600 MHz. (Bottom) Curves fitted to the $R_{1\rho}$ data with $R_2{}^0$ contributions removed, extended to the axes, and scaled arbitrarily along the *y*-axis for visualization. Note that the vertical ordering of the temperature is necessarily reversed between the two panels.

in R_2 for this resonance at very high ω_{eff} may be due to an inaccuracy in the measured R_1, which would lead to an ω_{eff}-dependent systematic error in R_2.

For the seven tetraloop resonances with measurable dispersion, the available CPMG and $R_{1\rho}$ data at both static field strengths were fit simultaneously assuming two-site exchange using eqs 3 and 4. The fitting of each of these resonances to the exchange equations gave a statistically significant improvement versus a description invoking ω_{eff}-independent rates (cumulative probability for F-statistic >0.95) except for G5 C4′ (0.91). In all cases, good agreement with all data was obtained using single values of k_{ex} and $p_a p_b(\Delta\omega)^2$, indicating consistency among the various data sets. Details of the fit procedure and a comprehensive tabulation of the resulting parameters are given in Supporting Information. For A7 C2′, it was necessary to invoke nonphysical values of $R_2{}^0$ and/or $R_{1\rho}{}^0$ to achieve a satisfactory fit; possible reasons are discussed below.

Table 2 reports k_{ex}, $(\Delta\omega)_{min}$, and $(\Delta\omega)_{est}$ values derived from dispersion data at 25 °C, where $(\Delta\omega)_{min}$, the minimum chemical shift change in ppm between the two exchanging conformations, is derived by assuming $p_a = p_b = 0.5$ and $(\Delta\omega)_{est}$ uses the estimated populations of C2′-endo and C3′-endo puckers from the *J*-coupling measurements of Jucker et al.[53] Throughout the tetraloop, two-state k_{ex} values ranging between 20,000 s^{-1} and 40,000 s^{-1} are observed, corresponding to exchange lifetimes τ_{ex} ($1/k_{ex}$) in the tens of microseconds. The CPMG data show no evidence of dramatic increases at high τ_{cp} (low ω_{eff}), as would be observed for exchange on timescales of milliseconds to tens of milliseconds.

The simplest molecular explanation for thermally activated exchange at ribose carbons is a transition between the C2′-endo and C3′-endo sugar ring conformations, although chemical-shift changes induced by nearby conformational shifts are also

Table 2. Motional Parameters at 25 °C Derived via Fitting of All Data for a Single Atom to Eqs 3 and 4

residue	atom	k_{ex}, s^{-1}	$(\Delta\omega)_{min}$, ppm[a]	$(\Delta\omega)_{est}$, ppm[b]	τ_{ex} (μs)
G5	C2′	$(2.5 \pm 0.3) \times 10^4$	0.90 ± 0.08	>1.26	41 ± 5
	C4′[c]	$(2.4 \pm 1.3) \times 10^4$	0.53 ± 0.20	>0.75	41 ± 22
C6	C2′	N/A	N/A	N/A	N/A
	C4′	$(3.4 \pm 0.4) \times 10^4$	2.28 ± 0.24	2.63 ± 0.28	29 ± 4
A7	C2′	$(4.0 \pm 0.6) \times 10^4$	3.42 ± 0.41	3.73 ± 0.44	25 ± 4
	C4′	$(3.5 \pm 0.4) \times 10^4$	1.98 ± 0.20	2.15 ± 0.22	29 ± 4
A8	C2′	$(2.2 \pm 0.3) \times 10^4$	0.91 ± 0.07	1.13 ± 0.09	46 ± 6
	C4′	$(2.5 \pm 0.4) \times 10^4$	1.07 ± 0.13	1.34 ± 0.17	40 ± 6

[a] Derived from $\Phi_{ex} = p_a p_b(\Delta\omega)^2$ using $p_a = p_b = 0.5$. [b] Derived by using estimates of C3′-endo pucker populations p_a of 0.75 for C6, 0.70 for A7, and 0.80 for A8, based on NMR *J*-coupling analysis.[53] For G5, *J*-coupling values were consistent with a fully C3′-endo population, and a lower bound for $\Delta\omega$ was thus derived, using $p_a > 0.85$. [c] Improvements in χ^2 using eqs 3 and 4 for this resonance did not reach statistical significance versus a constant relaxation rate model.

possible. In the present case, minimal chemical-shift changes spanning 0.5 ppm to almost 4 ppm are observed, consistent with the range of ^{13}C shifts predicted for pucker interconversions by density-functional calculations and solid-state NMR measurements.[79−81,91] For the three cases in which dispersion effects were observed for both C2′ and C4′ in a single residue (G5, A7, and A8), the exchange rate constants are identical within error between the two atoms. These two observations are consistent with the hypothesis that the observed relaxation dispersion effects throughout the tetraloop may be directly ascribed to two-state pucker interconversions of the corresponding ribose groups. For C6, the comparison between the two resonances could not be made, as dispersion effects were not observed for C2′. The lack of dispersion for C2′ may be due to an alternate source of chemical shift change for C4′ or simply due to a coincidence of chemical shifts of C2′ for the two pucker states (see Discussion). Under the presumption that observed dispersions for G5, A7, and A8 arise from C3′-endo/C2′-endo interconversions, therefore, we have performed combined fits for all data from C2′ and C4′ atoms on a given residue (dashed lines in Figure 5). The resulting motional parameters, reported in Table 3, fit the data very well and differ little from the results of the analyses of individual atoms.

The data in Tables 2 and 3 show the existence of two relatively tight clusters of exchange rates across multiple residues. Exchange rates for A7 C2′ and C4′ and G6 C4′ are all within error, although it can be noted that the values for the two C4′ atoms, at 3.4×10^4 s^{-1} $\pm$ 0.4×10^4 s^{-1} and 3.5×10^4 s^{-1} $\pm$ 0.4×10^4 s^{-1}, are much closer to each other than either is to A7 C2′ (4.0×10^4 s^{-1} $\pm$ 0.6×10^4 s^{-1}). For G5 and A8, all exchange rates fall into the narrow range of 2.2×10^4 s^{-1} to 2.5×10^4 s^{-1}. Since these clusters occur for a single data point, the correspondences could well be simply coincidental. Alternatively, the data may suggest the existence of two correlated dynamic processes, one affecting both apical residues and a second involving the entirety of the closing G-A base pair. To explore the possibility of coupled motion, we performed a global fit of all data for these two sets of resonances, representing overall totals of 14 and 21 data sets, respectively. In both cases, the resulting parameters fit the data very well and quantitatively track the corresponding individual analyses. The fitted curves are generally indistinguishable from those calculated at the individual or residue levels (dotted lines in Figure 5).

Temperature Dependence of Tetraloop Dynamics. To further probe the backbone dynamic properties of the GCAA tetraloop

(91) Rossi, P.; Harbison, G. S. *J. Magn. Reson.* **2001**, *151*, 1–8.

Table 3. Motional Parameters Derived from Simultaneous Fitting of C2′ and C4′ Data at 25 °C for Individual Residues or Combinations of Residues

Residue-Level Simultaneous Fits of Data for C2′ and C4′				
residue	k_{ex}, s^{-1}	$(\Delta\omega)_{min}$, C2′	$(\Delta\omega)_{min}$, C4′	τ_{ex} (μs)
G5	$(2.5 \pm 0.3) \times 10^4$	0.90 ± 0.08^a	0.54 ± 0.10	41 ± 5
C6 (C4′ only)[b]	$(3.4 \pm 0.4) \times 10^4$	N/A	2.28 ± 0.24	29 ± 4
A7	$(3.7 \pm 0.4) \times 10^4$	3.23 ± 0.24	2.10 ± 0.18	27 ± 3
A8	$(2.3 \pm 0.2) \times 10^4$	0.95 ± 0.07	1.02 ± 0.11	43 ± 4

Global Fit of All Data for C6 and A7					
k_{ex}, s^{-1}	$(\Delta\omega)_{min}$, C6 C2′	$(\Delta\omega)_{min}$, C6 C4′	$(\Delta\omega)_{min}$, A7 C2′	$(\Delta\omega)_{min}$, A7 C4′	τ_{ex} (μs)
$(3.3 \pm 0.2) \times 10^4$	N/A	2.35 ± 0.09	3.01 ± 0.14	1.92 ± 0.10	30 ± 2

Global fit of all data for G5 and A8					
k_{ex}, s^{-1}	$(\Delta\omega)_{min}$, G5 C2′	$(\Delta\omega)_{min}$, G5 C4′	$(\Delta\omega)_{min}$, A8 C2′	$(\Delta\omega)_{min}$, A8 C4′	τ_{ex} (μs)
$(2.4 \pm 0.2) \times 10^4$	0.87 ± 0.05	0.52 ± 0.09	0.96 ± 0.06	1.04 ± 0.10	42 ± 3

[a] All $\Delta\omega$ values in ppm. [b] Reproduced from Table 2 to facilitate comparison.

Table 4. Temperature Dependence of Exchange Parameters for Single Resonances

resonance	k_{ex} (15 °C), s^{-1}	k_{ex} (20 °C), s^{-1}	k_{ex} (25 °C)^a, s^{-1}	k_{ex} (35 °C), s^{-1}	E_a, kJ/mol
G5 C2′	$(1.2 \pm 0.1) \times 10^4$	$(1.3 \pm 0.6) \times 10^4$	$(2.5 \pm 0.3) \times 10^4$	nd	nd
G5 C4′	$(1.6 \pm 0.2) \times 10^4$	$(1.9 \pm 1.8) \times 10^4$	$(2.4 \pm 1.3) \times 10^4$	nd	nd
C6 C4′	$(1.1 \pm 0.1) \times 10^4$	$(1.9 \pm 0.4) \times 10^4$	$(3.4 \pm 0.4) \times 10^4$	nd	74 ± 10
A7 C2′	$(2.0 \pm 0.4) \times 10^4$	$(2.2 \pm 0.3) \times 10^4$	$(4.0 \pm 0.6) \times 10^4$	$(7.0 \pm 2.4) \times 10^4$	50 ± 12
A7 C4′	$(1.3 \pm 0.2) \times 10^4$	$(1.7 \pm 0.5) \times 10^4$	$(3.5 \pm 0.4) \times 10^4$	$(7.3 \pm 2.5) \times 10^4$	72 ± 13
A8 C2′	$(1.4 \pm 0.1) \times 10^4$	$(1.3 \pm 1.4) \times 10^4$	$(2.2 \pm 0.3) \times 10^4$	nd	31 ± 11
A8 C4′	$(1.4 \pm 0.3) \times 10^4$	$(1.5 \pm 1.5) \times 10^4$	$(2.5 \pm 0.4) \times 10^4$	nd	40 ± 18

[a] Reproduced from Table 2 to facilitate comparison.

and the possible correlations among observed motions, we repeated a subset of the spin relaxation analyses at 600 MHz and 15 °C, 20 °C, and 35 °C. A summary of the results obtained is collected in Table 4. In general, Φ_{ex} shows little or no temperature dependence within the experimental error, implying that the shift in the populations of the exchanging states is insufficient to cause dramatic changes in the product $p_a p_b$ (Supporting Information). By contrast, a sharp dependence of k_{ex} with temperature is seen, consistent with the thermally activated nature of the conformational exchange process. The quantitative patterns of k_{ex} values for various residues are somewhat different as the temperature is varied. For G5 and especially for A7, the agreement between k_{ex} for C2′ and C4′ atoms worsens as the temperature is lowered, although the differences are not dramatically outside the estimated errors. At 35 °C, reliable data could only be obtained for A7 C2′ and A7 C4′, and the k_{ex} values for these resonances agree within error.

For the C4′ resonance of residue A7, CPMG and $R_{1\rho}$ relaxation dispersion data along with best-fit curves for three different temperatures are shown in Figure 6. The most prominent feature of the data is the consistent and substantial decrease in the magnitude of R_{ex} with temperature, which arises from the scaling of eqs 3 and 4 by $1/k_{ex}$ for $k_{ex} \geq \omega_{eff}$. This effect gives rise to the lower limit of the time scale that relaxation dispersion data can analyze. In our case, exchange faster than ~10 μs would result in an R_{ex} term too small to be visible at 600 MHz even for a relatively large Φ_{ex}. The use of ultrahigh static fields extends this limit when such data are available. To display the effect of varying k_{ex} on the shape of the data independent of the magnitude of $R_{ex}^{\omega_{eff}\to 0}$, Figure 6b shows the fitted curves to the $R_{1\rho}$ data from panel a in Figure 6 extrapolated to the y-axis and scaled arbitrarily to identical values at $\omega_1 = 0$. (The lower range of this extrapolation is nonphysical even could the data be obtained, as the functional form of the $R_{1\rho}$ dispersion curve alters outside of the slow-exchange limit. We include this section of the curve solely to aid visualization.)[92,93] As seen in the simulated data sets (Supporting Information, Figure S1), the inflection point of the dispersion curve shifts smoothly to higher ω_1 with temperature. The magnitude of this shift directly reflects the temperature dependence of k_{ex} and thus the activation barrier for the exchange process.

The k_{ex} parameter extracted from dispersion data is not itself a fundamental rate constant but is the sum of the forward and reverse rate constants for the exchange process. In the absence of knowledge of the temperature-dependent populations of the two states, the individual rates k_1 and k_{-1} cannot be extracted in the fast-exchange limit operative here, and a rigorous thermal analysis cannot be performed. Nevertheless, an Arrhenius-type plot of ln k_{ex} vs $1/T$ yields a phenomenological activation energy that is broadly characteristic of the thermal barrier for the process and has been useful for comparisons in other systems.[94] Arrhenius-type plots for ribose resonances in the apical nucleotides of GCAA are shown in Figure 7, and resulting E_a values are collected in Table 4. Results for G5 showed large errors due to the small R_{ex} values at 600 MHz and are not reported. Activation energies at other sites ranged between ~40 kJ/mol and ~75 kJ/mol.

For A8, E_a agrees well between the C2′ and C4′ atoms, as does k_{ex} at each temperature analyzed, strongly supporting our interpretation that the observed dispersion at this residue arises from a single conformational equilibrium affecting both C2′ and

(92) Trott, O.; Palmer, A. G. *J. Magn. Reson.* **2002**, *154*, 157–160.
(93) Korzhnev, D. M.; Orekhov, V. Y.; Dahlquist, F. W.; Kay, L. E. *J. Biomol. NMR* **2003**, *26*, 39–48.
(94) Kovrigin, E. L.; Cole, R.; Loria, J. P. *Biochemistry* **2003**, *42*, 5279–5291.

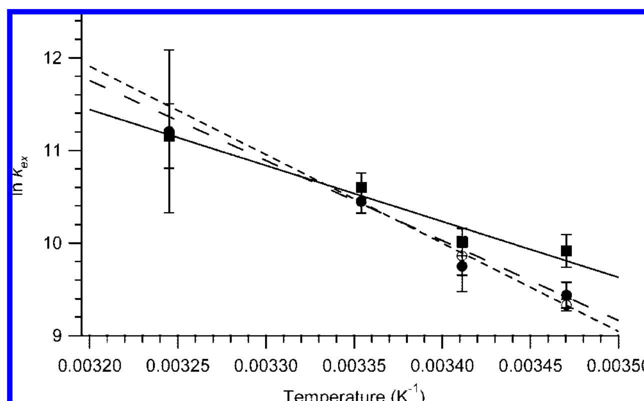

Figure 7. Arrhenius-type plots of the exchange rate constant k_{ex} for C6 C4′ (open circles, short dash), A7 C2′ (filled squares, solid line), and A7 C4′ (filled circles, long dash). Results for C6 C4′ were not available at 35 °C (smallest 1/*T* value).

C4′ sites. We ascribe these dynamics to C3′-endo/C2′-endo repuckering transitions. The relatively poorly determined data for G5 C2′ and C4′ at lower temperatures also agree very well with the two A8 resonances. For C6 and A7, the situation is somewhat more complex (Figure 7). The correlation between exchange rates at C6 C4′ and A7 C4′ discussed above continues at all observed temperatures, leading to essentially identical E_a values. In contrast, the thermal analysis appears to suggest that a separate exchange process exists, affecting A7 C2′ but not A7 C4′, with the agreement at 25 °C representing the temperature at which the two lines cross.

Activation energies measured here for the GCAA tetraloop are intriguingly large compared both to individual biomolecular interactions and to results in other systems. For example, in backbone ^{15}N relaxation studies in RNase A, the two resonances giving reliable results yielded activation energies for exchange of 15 and 31 kJ/mol.[95] These values are noticeably smaller than those observed here, even though the dynamic process in question was interpreted as involving a substantial fraction of the protein structure. Estimates of activation barriers to pseudorotation in furanose rings and nucleosides vary between ~6 kJ/mol and ~20 kJ/mol,[96−100] and the barrier heights for furanose dynamics in the DNA *Hha*I binding site were found by 2″-^{2}H solid-state NMR line shape analysis to be 11−15 kJ/mol,[86] implying a substantial increase in barrier height for pseudorotation in GCAA due to the structural context of the tetraloop. Relatively large values for E_a in the tetraloop are consistent with the substantial number of stacking and hydrogen-bonding interactions within GNRA tetraloops as well as with models in which dispersion arises from correlated fluctuations involving multiple nucleotides (see below).

Discussion

Along with the phosphodiester linkages and nucleotide base side chains, backbone ribose groups are a principal component of nucleic acid structures. The conformations of these groups are dominated by the equilibrium between the C3′-endo and C2′-endo pseudorotation conformations (Scheme 1), and the equilibrium between these forms is a key discriminator between A-form and B-form helices as well as among various nonhelical structures.[41,42] Heretofore, the powerful technique of probing biomolecular dynamics with heteronuclear NMR spin relaxation studies has largely been limited in RNA to side chain ^{13}C and ^{15}N groups and, in favorable cases, anomeric C1′ atoms.[27] Anomeric carbons are expected to display a relatively small chemical shift change upon pucker interconversion, however, rendering these resonances an insensitive probe of μs−ms scale exchange between C3′- and C2′-endo conformers.[80,81] The use of alternate-site labeling to allow relaxation dispersion studies of C2′ and C4′ resonances therefore provides a unique methodology for probing sugar pucker dynamics within structured RNA molecules.

In this work, we report a comprehensive spin-relaxation analysis of C2′ and C4′ ribose carbon atoms in the GCAA tetraloop. At 25 °C, loop ribose groups are largely rigid at the subnanosecond time scale. At longer timescales, in contrast, we find an extensive network of conformational exchange processes throughout the tetraloop. Figure 8 shows the high-resolution crystal structure of a closely related GUAA tetraloop[59] with CPK spheres shown proportional to $(\Delta\omega)_{min}$ for the corresponding resonance. These results draw a picture of a set of relatively well-defined backbone conformations that interconvert over tens of microseconds. In some cases, ribose dynamics appear to be more extensive than those sensed by nucleotide bases (see below), and thus may suggest the existence of backbone reorientations occurring with relatively little disruption of the stacking of the nucleotide bases. An important caveat is that the methods used here will not detect dynamics between the two windows probed by model-free and relaxation dispersion analyses, i.e., on the time scale of tens to hundreds of nanoseconds. Recently developed ^{2}H solid-state NMR methods have the potential to fill this gap by providing dynamic information spanning the ns−μs time scale.[86,101−103] By contrast, solution-state ^{2}H NMR of specifically labeled samples[33,34] provides a valuable complementary probe of fast side-chain dynamics, but is expected to be relatively insensitive to the μs−ms motions of greatest interest here.

An important question in the analysis of molecular motion is the extent to which dynamics at different sites are correlated, that is, whether the local conformations observed at different atoms are coupled or independent. Conventional NMR spin relaxation experiments do not directly probe the correlation between the motions of different bond vectors, but a coincidence of exchange rate constants, especially if maintained across a range of temperatures or other conditions, can provide suggestive evidence for coupled motion. At 25 °C, all residues for which dispersion profiles could be evaluated for both C2′ and C4′ (G5, A7, and A8) show identical k_{ex} values within error between the two resonances, consistent with a simple model in which the observed dynamics correlate with repuckering events for the individual sugars. This correlation may be lost

(95) Cole, R.; Loria, J. P. *Biochemistry* **2002**, *41*, 6072–6081.
(96) Olson, W. K.; Sussman, J. L. *J. Am. Chem. Soc.* **1982**, *104*, 270–278.
(97) Olson, W. K. *J. Am. Chem. Soc.* **1982**, *104*, 278–286.
(98) Harvey, S. C.; Prabhakaran, M. *J. Am. Chem. Soc.* **1986**, *108*, 6128–6136.
(99) Roder, O.; Ludemann, H. D.; Vongoldammer, E. *Eur. J. Biochem.* **1975**, *53*, 517–524.
(100) Foloppe, N.; Nilsson, L.; MacKerell, A. D. *Biopolymers* **2001**, *61*, 61–76.
(101) Miller, P. A.; Shajani, Z.; Meints, G. A.; Caplow, D.; Goobes, G.; Varani, G.; Drobny, G. P. *J. Am. Chem. Soc.* **2006**, *128*, 15970–15971.
(102) Olsen, G. L.; Echodu, D. C.; Shajani, Z.; Bardaro, M. F., Jr.; Varani, G.; Drobny, G. P. *J. Am. Chem. Soc.* **2008**, *130*, 2896–2897.
(103) Pederson, K.; Meints, G. A.; Shajani, Z.; Miller, P. A.; Drobny, G. P. *J. Am. Chem. Soc.* **2008**, *130*, 9072–9079.

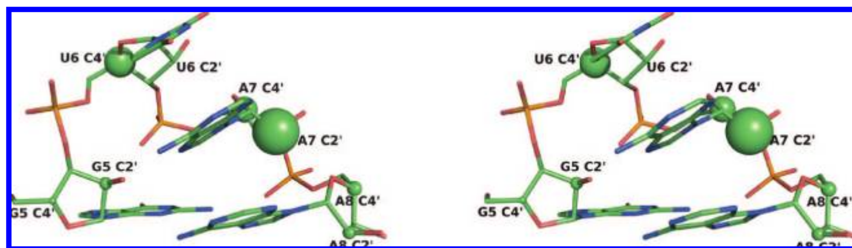

Figure 8. Crystal structure of the GUAA tetraloop determined at 1.4 Å resolution by Correll and Swinger (PDB code 1MSY).[59] CPK spheres for C2′ and C4′ atoms are drawn with radii proportional to $(\Delta\omega)_{min}$ values for the corresponding resonances in the GCAA variant.

at lower temperatures in the cases of A7 and G5, although the errors in the latter case are substantial (Table 4). It should be noted that data at multiple static fields are only available at 25 °C. Extracted parameters at other temperatures may be less accurate, especially for low R_{ex}. On the other hand, increased complexity of exchange processes at lower temperatures has been previously observed in protein-folding studies and ascribed to deviations from a two-state model as the temperature drops.[104] Above the nucleotide level, individual and residue fits show that k_{ex} values fall into two relatively narrow clusters, one characteristic of the closing G5-A8 base pair and the other characteristic of the apical C6 and A7 residues, perhaps suggesting a correlation of motions across these two broad regions of the tetraloop. A similar clustering of exchange constants across neighboring nucleotides has previously been observed in the internal stem loop of the U6 snRNA.[24] Widespread correlated motions in the GCAA system could help explain the relatively high activation energies encountered here compared to estimates for repuckering of single nucleotides. Analysis of dispersion curves assuming a single process affecting both C2′ and C4′ atoms within a single ribose sugar or spanning multiple nucleotides of the tetraloop resulted in fits essentially indistinguishable from the individual or residue-level analyses (Table 3; Figure 5).

The above interpretation of correlated motion is based on the premise that dynamics transitions of ribose rings are dominated by sugar pucker conversions. Nucleotide C6 appears to violate this assumption, however, as dispersion is observed for the C4′ but not the C2′ resonance (Figure 5c,d). There are two possible explanations for this apparent discrepancy. First, eqs 3 and 4 show that the magnitude of R_{ex} is dependent on the square of the chemical shift change between the exchanging states, $(\Delta\omega)^2$. Atoms that are affected by a conformational exchange but happen to have very similar chemical shifts in the two states, therefore, will show little or no relaxation dispersion. A very small chemical shift change upon pucker conversion under some circumstances is compatible with DFT predictions for ribose carbons.[80,81] The lack of dispersion at C6 C2′, therefore, provides no independent evidence that the dispersion at C6 C4′ arises from repuckering of the corresponding ribose, but also does not directly contradict it. (The observation of exchange contributions with different k_{ex} at two resonances for a given sugar, by contrast, would immediately rule out pucker equilibrium as the sole source for R_{ex} at those sites; we do not observe this effect at any of the four tetraloop nucleotides). The second possibility is that the pucker conformation of C6 in fact does not interconvert on the time scale probed by the current experiments, but the observed dispersion of C6 C4′ instead arises from some other process. Given the close correspondence between the temperature-dependent behavior of C6 C4′ and A7 C4′, this is likely to arise from a motion centered on the pucker equilibrium of A7. The chemical shift of C6 C4′ would then change with repuckering of A7 either via a coupled reorientation of the backbone in this region or via an alteration of the local environment of C6 C4′ due solely to conformational equilibria at the neighboring residue A7, with the conformation at C6 undergoing little or no change.

Scalar couplings for C6 clearly indicate that the nucleotide exists in equilibrium between C3′-endo and C2′-endo conformations, implying that C3′-endo/C2′-endo conversions should be detectable for this residue.[52] Since C6 is the least structurally constrained of the four tetraloop nucleotides, however (Figures 1 and 8), its pucker equilibrium could very well be established on a fast time scale compared to other nucleotides in the loop (i.e., sub-μs), and thus be observed by neither relaxation dispersion nor fast-dynamics experiments. Consistent with this idea, comparisons of solution-state ^{13}C relaxation with solid-state NMR data have allowed the identification of motions on the sub-μs time scale in the TAR element from HIV-1.[102]

Insight into the possible physical sources of observed dynamics may be provided by comparison with structural, thermodynamic, and calculational studies. The apical residues C6 C4′ and A7 C4′, which are connected by the highly constrained backbone in this region of the structure, show substantial R_{ex} contributions with essentially identical k_{ex} and E_a values (Table 4; Figure 7). By contrast, relaxation-dispersion studies of the GAAA tetraloop in the context of the lead-dependent ribozyme found little evidence for R_{ex} processes affecting the side chains of these two residues.[20] Model-free analysis of nucleotide base ^{13}C atoms in the GCAA tetraloop found that an R_{ex} term was not required for data fitting of carbon-6 of C6 or either protonated carbon on A7, but was necessary for carbon-5 of C6. The latter result was ascribed to interconversion between the two states of the cytosine base observed in the NMR structure (Figure 1).[60] A subset of 10-ns molecular dynamics calculations on the GCAA system showed excursions to a conformation in which the destacking of base C6 is coupled to a C3′-endo/C2′-endo transition at the same nucleotide.[55] The sugar pucker of C6 was also inverted to C2′-endo in the two members of the NMR structure family that displayed unstacked conformations for the corresponding base (Figure 1).[53] A unified explanation for this data would be that a backbone reorientation coupled to the loss of C6-A7 stacking gives rise to the observed dispersion at both C6 4′ and A7 4′. In the GAAA tetraloop, this process may be fully or partially quenched by the stronger stacking interaction of A7 with a purine at position 6.[20,53]

The thermal analysis of exchange rates hints at the existence of multisite exchange at the A7 C2′ site, since k_{ex} values for this resonance diverge somewhat from those of C6 C4′ and A7 C4′ at lower temperatures. In addition, difficulties in data

(104) Korzhnev, D. M.; Salvatella, X.; Vendruscolo, M.; Di Nardo, A. A.; Davidson, A. R.; Dobson, C. M.; Kay, L. E. *Nature* **2004**, *430*, 586–590.

analysis within the two-state model were encountered for A7 C2′, including the necessity to invoke nonphysical values of R_2^0 or $R_{1\rho}^0$ (Supporting Information) and apparent inconsistencies between the CPMG and $R_{1\rho}$ data at 15 °C. The latter observations are consistent with the need for a more complex model to describe the dynamics at this site, although experimental difficulties in the presence of very large exchange contributions cannot be ruled out. If A7 C2′ does indeed sample more than two states, the simplest explanation is that the C3′-endo/C2′-endo equilibrium at residue 7 gives rise to the dispersion at A7 C4′ and contributes to that at A7 C2′, whereas a second process with a distinct rate constant further modulates the chemical shift of A7 C2′ only. Extrusion of the base of A8 could potentially play such a role by modulating the chemical shift of A7 C2′. Unfortunately, given the absence of reliable data for A7 C2′ at the higher field strength used, the current data set is insufficient for analysis in terms of a multisite exchange model.

Within the limited precision of the data, the exchange rates for all four ribose resonances in the loop-closing G5-A8 base pair coincide at the three temperatures analyzed (Table 4; Figure 7). If this correspondence is genuine, it raises the possibility of a coupled dynamic process spanning the full width of this base pair. In the GAAA tetraloop in the context of the leadzyme, exchange dynamics were observed at C8 and C2 of the A8 base, but not at A8 of G5.[20] This result was ascribed to the dynamic exchange of hydrogen bonding partners suggested earlier by thermodynamic and structural studies.[51,53] In the model-free analysis of base ^{13}C resonances in GCAA, strong exchange contributions were observed at A8 C2, with no data obtained for A8 C8, consistent with this exchange being maintained in the case of GCAA.[60] In tetraloop structures, these two nucleotides are interconnected by an intricate network of hydrogen-bonding interactions, making coupled dynamics plausible. Of particular interest, comparative NMR studies uncovered a potential hydrogen-bonding interaction between the amino group of A8 and the 2′-OH of G5 that was present in the GAGA tetraloop but not in the GCAA variant studied here.[53] An appealing hypothesis is thus that the GCAA tetraloop could sample a minor conformation resembling the most stable conformation for GAGA, including formation of the A8 amino-G5 2′-OH hydrogen bond, resulting in the relaxation dispersion effects observed throughout the closing base pair. If individual tetraloop species can indeed sample hydrogen-bonding patterns characteristic of different sequences, the formation and breakage of hydrogen bonds of this type provides a potential mechanism for the coupling of motions of the A8 base and the G5 sugar.

Another possibility for the molecular nature of the G5-A8 dynamic transition is a more extensive local disruption of the tetraloop structure itself. Molecular dynamics simulations of GCAA at 400 K displayed sampling of a low-probability conformation in which the A8 base is extended from the loop in obligatory coupling with a C3′-endo/C2′-endo conversion of the same sugar; this coupling was not observed on available timescales for simulations at 300 K.[55] Interestingly, both molecular dynamics simulations and *J*-coupling measurements indicated a greater fraction of minor conformations existing for the apical nucleotides than for the closing base pair, consistent with the relative $p_a p_b(\Delta\omega)^2$ values observed here (Supporting Information; Figure 8).

Taken together, the results presented here illustrate the power of ^{13}C spin relaxation experiments on the ribose backbone to open a new vista on the dynamic properties of RNA systems. The preparation of the labeled nucleotides that enable this work entails straightforward modifications of standard growth procedures rather than detailed chemical or enzymatic synthesis, minimizing the additional time and effort required.[36,105] As the size of RNA systems of interest increases, spectral resolution within the relatively poorly dispersed ribose regions of two-dimensional spectra will be an increasing concern. The collapse of ^{13}C multiplet structure will noticeably reduce spectral overlap in nonconstant time spectra. In addition, as in the present case, resonances of particular interest will often lie in regions of noncanonical structure and thus be better dispersed than helical regions (Figure 2). The techniques of nucleotide-selective and segmental isotope labeling can further increase the range of applicability of the technique.[106−111] The quality of the data obtained is illustrated in GCAA by the ability to simultaneously fit multiple types of data at two static fields, in some cases across numerous resonances.

For the GNRA tetraloop system, perhaps the most useful source of physical insight arises from the combination of the backbone ^{13}C relaxation dispersion studies with the wealth of previous biochemical and biophysical data in this system. The comparison of NMR data with molecular dynamics simulations is a particularly powerful and generally applicable technique.[29,30] For systems such as ribozymes and protein-binding RNAs, further insight may be obtained via comparisons with probes of the importance of ribose structure and dynamics for molecular function.[112] Especially for larger, multidomain systems, the technology of NMR residual dipolar coupling analysis can provide a further source of detailed information.[113,114]

Conclusions

NMR spin relaxation dispersion in combination with metabolically directed specific labeling of C2′ and C4′ atoms has proven to be an effective probe of conformational dynamics in the RNA ribose ring. This technology yields a novel type of information complementary to previously applied NMR spin relaxation experiments on nucleotide base side chains and anomeric carbon atoms. In the well-studied GCAA tetraloop, we have obtained a detailed picture of a set of individually well-defined backbone conformations, connected by exchange processes that appear to be centered on the pucker equilibria of adjoining nucleotides. The combined use of spectroscopic, biochemical, and calculational probes has the potential to yield true “dynamics−function” studies in RNA−ligand recognition and ribozyme catalysis, and thus to provide unique and powerful insight into these fascinating systems.

(105) Hoogstraten, C. G.; Johnson, J. E., Jr. *Concepts Magn. Reson. Part A* **2008**, *32*, 34–55.
(106) Xu, J.; Lapham, J.; Crothers, D. M. *Proc. Natl. Acad. Sci. U.S.A.* **1996**, *93*, 44–48.
(107) Kim, I.; Lukavsky, P. J.; Puglisi, J. D. *J. Am. Chem. Soc.* **2002**, *124*, 9338–9339.
(108) Peterson, R. D.; Theimer, C. A.; Wu, H.; Feigon, J. *J. Biomol. NMR* **2004**, *28*, 59–67.
(109) Tzakos, A. G.; Easton, L. E.; Lukavsky, P. J. *J. Am. Chem. Soc.* **2006**, *128*, 13344–13345.
(110) Tzakos, A. G.; Easton, L. E.; Lukavsky, P. J. *Nat. Protoc.* **2007**, *2*, 2139–2147.
(111) Nelissen, F. H.; van Gammeren, A. J.; Tessari, M.; Girard, F. C.; Heus, H. A.; Wijmenga, S. S. *Nucleic Acids Res.* **2008**, *36*, e89.
(112) Julien, K. R.; Sumita, M.; Chen, P.-H.; Laird-Offringa, I. A.; Hoogstraten, C. G. *RNA* **2008**, *14*, 1632–1643.
(113) Al-Hashimi, H. M. *ChemBioChem* **2005**, *6*, 1506–1519.
(114) Getz, M.; Sun, X.; Casiano-Negroni, A.; Zhang, Q.; Al-Hashimi, H. M. *Biopolymers* **2007**, *86*, 384–402.

Acknowledgment. This research was supported by NIH Grant GM069742 to C.G.H. and NIH Ruth L. Kirschstein Predoctoral Fellowship GM075735 to J.E.J. The work made use of a Bruker AVANCE 900 MHz NMR spectrometer funded by the Michigan Economic Development Corporation and Michigan State University as well as equipment in MSU's Max T. Rogers NMR Facility. We are grateful to J. Patrick Loria for helpful discussions, to Kristine Julien for technical support, and to Kermit Johnson, Daniel Holmes, and Aizhuo Liu for assistance with data collection.

Supporting Information Available: A detailed description of the data fitting and parameters used in the analysis of relaxation dispersion data and six tables reporting the full results of this analysis. A discussion of the useful ranges of the various experimental schemes and one figure showing sets of simulated dispersion data for different exchange rates.This material is available free of charge via the Internet at http://pubs.acs.org.

JA805759Z